Journal of Magnetic Resonance **140,** 172–178 (1999)
Article ID jmre.1999.1811, available online at http://www.idealibrary.com on IDEAL®

High-Resolution Magnetic Relaxation Dispersion Measurements of Solute Spin Probes Using a Dual-Magnet System

Shawn Wagner, Timothy R. J. Dinesen, Timothy Rayner, and Robert G. Bryant[1]

Chemistry Department, University of Virginia, Charlottesville, Virginia 22901

Received December 24, 1998; revised May 5, 1999

The magnetic field dependence of the nuclear spin–lattice relaxation rate provides a detailed report of the spectral density functions that characterize the intra- and intermolecular fluctuations that drive magnetic relaxation. We have addressed the difficult sensitivity and resolution problems associated with low magnetic field strengths by using two magnets in close proximity and shielded from each other. The sample is stored in the high magnetic field, pneumatically driven to the variable satellite field, then returned to the high field for detection at high resolution. A magnetic shield effectively decouples the two magnets so that varying the satellite field strength has minimal effect on the field strength and shim of the high field magnet. The disadvantage of the sample–shuttle magnet-pair system is the restriction imposed on the relaxation times by the finite shuttle times. Experiments not described here have shown this rate maximum to be about 20 s^{-1} for most practical solutions. However, we demonstrate here that the sensitivity gains over switched-current magnet systems permit characterization of solute inter- and intramolecular dynamics over the time scale range from tens of microseconds to less than a picosecond. This range permits investigation of a number of crucial chemical dynamics questions, while high sensitivity permits examination of a variety of solute spins. Representative data are presented for ^{1}H, ^{111}Cd, and ^{7}Li.

Key Words: **high-resolution magnetic relaxation dispersion; magnetic relaxation dispersion; nuclear magnetic relaxation dispersion; field dependence; spin–lattice relaxation.**

INTRODUCTION

Problems ranging from molecular recognition to chemical reactivity can be discussed within the context of molecular dynamics that include the concerted intramolecular modes and solute diffusion properties. The magnetic field dependence of nuclear spin–lattice relaxation rates known as the magnetic relaxation dispersion (MRD) maps the spectral density functions that are Fourier transforms of the correlation functions that characterize such random molecular motions. In principle, the relaxation dispersion data provide virtually all the dynamical information relevant to a nuclear magnetic resonance experiment, provided that a sufficiently wide range of magnetic field strengths is sampled. The S/N and spectral resolution of an NMR experiment are both field dependent, so varying the magnetic field of the spectrometer for the purpose of measuring the spectral density presents problems at low fields (*1, 2*). A solution to the sensitivity problem is to induce time dependence in magnetic field strength either by varying the current in a superconducting solenoid or resistive electromagnet or by physically moving the sample between two independent fields. Switched-current systems have the advantage of short field-switch times, which allow measurement of high relaxation rates (*3–6*). However, the magnetic field strengths achieved imply low sensitivity, and resolution is that associated with a minimally shimmed magnet. Spectrometer arrangements in which time dependence of the magnetic field is derived from physical sample displacement have been employed extensively to execute zero-field NMR (*7*) and pure nuclear quadrupole resonance (*8, 9*). Utilization of a well-shimmed high field magnet provides vastly improved sensitivity and spectral resolution as compared with switch-current magnets. The range of observable relaxation rates is limited in this setup by the finite time for the sample transit, since relaxation occurring in the region between the two principal magnetic fields cannot be easily controlled.

In this paper, we describe a dual magnet arrangement in which the sample is shuttled pneumatically between independent fields to record the magnetic field dependence of the nuclear spin–lattice relaxation rates. In the configuration implemented, the two magnetic fields are sufficiently well isolated that good resolution is maintained in the high field while the satellite field is changed over the range from 0 to 1.6 T. We demonstrate the capabilities of the approach with magnetic relaxation dispersion measurements of ^{1}H, ^{111}Cd, and ^{7}Li.

MAGNETIC FIELD CYCLE AND SAMPLE MOVEMENT

The magnetic field pair consists of a 7.05-T 65-mm-bore superconducting magnet located 231 mm above a 1.25-cm-thick iron box housing a GMW Model 3472-70 10.16 cm electromagnet (Fig. 1). The electromagnet is orthogonal to the superconducting magnet field, resulting in only a 0.23-ppm change in field strength (Fig. 2) when the electromagnet is used

[1] To whom correspondence should be addressed. Fax: (804) 924–3567. E-mail: rgb4g@virginia.edu.

1090-7807/99 $30.00

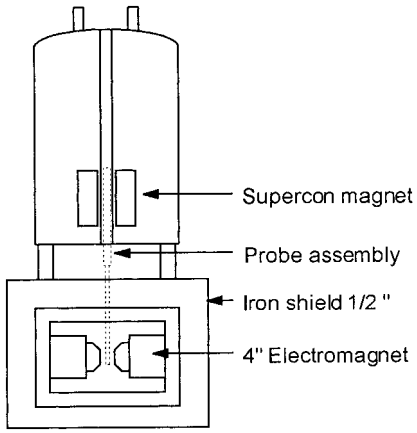

FIG. 1. Schematic representation of the magnet pair system consisting of the 7.05-T superconducting magnet, which provides the preparation and detection field, and the variable-field electromagnet inside the shield, which provides the evolution field in which relaxation is studied. The sample is pneumatically moved from the preparation field to the evolution field, where it resides for a variable time, then is pneumatically moved back to the detection field, where the magnetization is sampled by a standard RF pulse sequence period.

at its maximum field of 1.6 T at a pole gap of 19 mm. The electromagnet is driven by a Danyfysik System 8000 power supply with 18-bit current resolution, providing a stable magnet field. Regulation of the variable magnet field is controlled by an EPS 386 personal computer running Labview 4.1. The magnetic field is sensed by a Hall Probe affixed to the pole piece and is coupled to the computer via a GPIB PCII interface and a DTM-141 Digital Teslameter. The spectrometer is controlled by a Macintosh Quadra 800 computer using a Libra Tecmag unit which provides TTL outputs and a digital data acquisition board. The Macintosh computer runs Tecmag MacNMR and Applescript. This combination of software permits facile pulse sequence programing, data storage, sample movement, and control of the satellite electromagnet field settings.

Pneumatic control of the sample employs TTL lines from the Tecmag Libra system which are interfaced through a low current LED and a 2N2222 transistor to a Potter & Brumfield ODC-5 solid-state relay (Fig. 3). The LED both provides a visual indicator of the active TTL line and functions as a 100-kΩ resistor to limit current flow. These relays drive an SMC NVS4314-00520 dc air value solenoid for the sample up/down pressure or an SMC NVS4114-00520 dc air valve solenoid for the sample locking pins that minimize sample bounce as discussed below. A dual solenoid without a spring return is used to control the sample position, which minimizes solenoid heating because the current need not be persistent to hold the solenoid on. A single solenoid using a spring return is used for the antibounce sample locking pins. Air pressure typically used to move the sample is 0.4 atm above atmospheric pressure and typical transit times between fields are 100 ms with this design.

Isolation of the two magnet fields was achieved by enclosing the variable-field electromagnet in an iron box designed by Magnex Corporation. The forces developed by the interaction

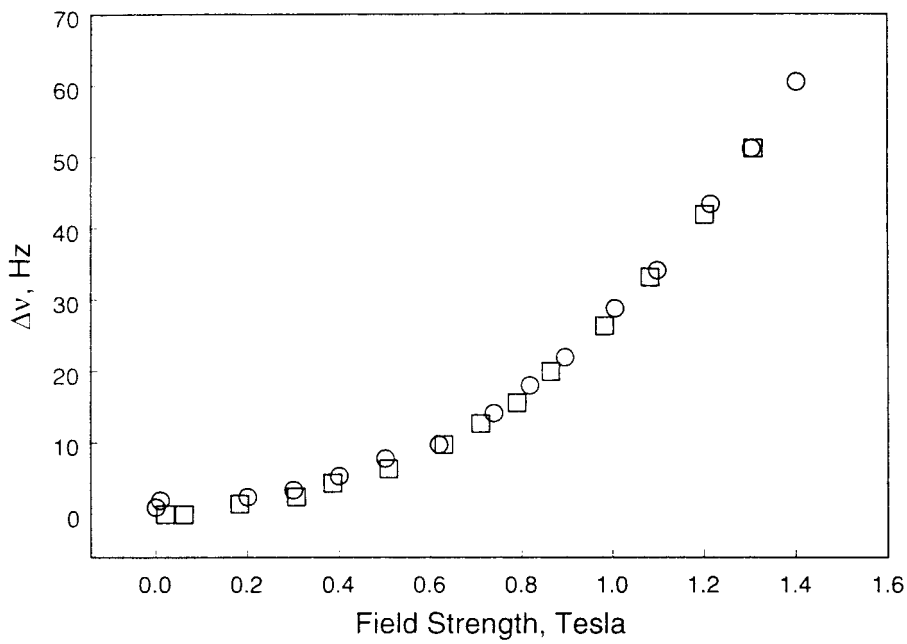

FIG. 2. Change in the resonance frequency of the water proton resonance measured in the high or detection field as a function of the field setting in the satellite evolution field. The circles were recorded when the satellite field was increased, while the squares were recorded when the satellite field was decreased from the maximum value.

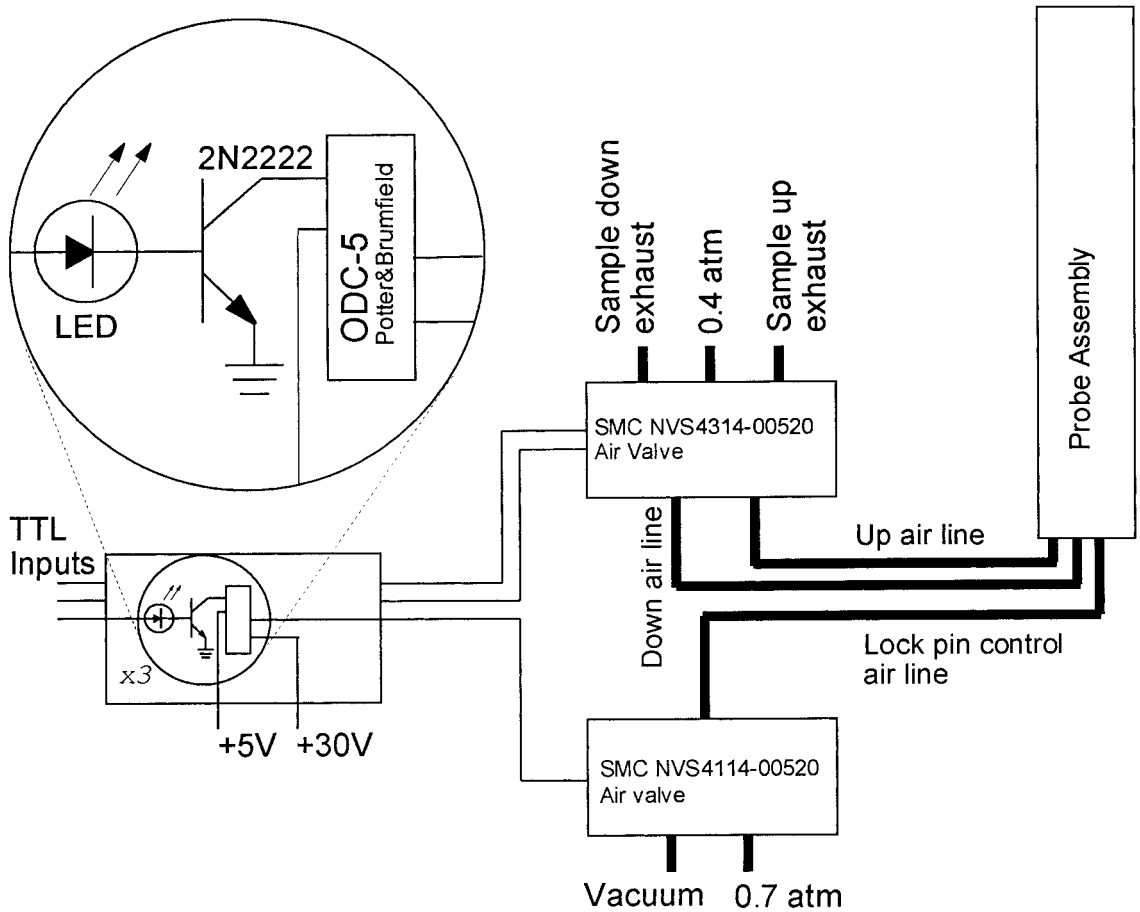

FIG. 3. Schematic diagram of the sample shuttle control arrangement. The 2N2222 transistors buffer the TTL logic pulse which drives the Potter & Brumfield, ODC-5 solid-state relays.

between the iron shield and the superconducting magnet require modification of the magnet support structure internal to the Dewar to handle the stresses, which was also designed by Magnex. A 11.7-T Dewar was used to provide a larger helium capacity to increase the cryogen hold times. Access to the electromagnet compartment is provided by a 26 × 29-cm sliding iron door. Service cables providing water, electricity, air, and vacuum are provided by 35 × 56-mm ports at the bottom of the iron shield. The sample shuttle tube is admitted to the shielded region through a 1.0-cm hole that is directly below the superconducting magnet bore. This configuration results in a distance of 82 cm between the two magnetic field centers.

THE LIQUID SAMPLE SHUTTLE

The sample container must satisfy conflicting requirements of minimal mass, maximum detection volume, and mechanical strength sufficient to suffer tens of thousands of rapid accelerations and decelerations while containing a liquid sample. Although different approaches may be adequate, we find that the design indicated in Fig. 4 works well. The sample container or shuttle is made of Delrin, with the liquid confined in the smaller-diameter end. The thin walls at this end permit maximal coupling between the RF coil and the sample. The thin walls are mechanically adequate because the stresses of the sudden stop in the detection region are taken largely by the stop shoulders where the shuttle has thick walls. The liquid is confined by insertion of a silicone O-ring cord stock piece and subsequent compression by a threaded nylon rod that is cut flush with the outer wall of the shuttle. The sample volume is approximately 0.20 ml, which is smaller than normal for high-resolution spectroscopy. The small volume has several obvious implications: The NMR signal is reduced. The small mass reduces the settling and transit times. The high degree of field homogeneity with standard field shims is lost because of the small sample diameter. The resolution is still sufficient, however, for most experiments of interest. The sensitivity loss caused by the small diameter cannot be easily regained by simply increasing the diameter of the shuttle. In many cases spin–lattice relaxation rates are large, resulting in large signal

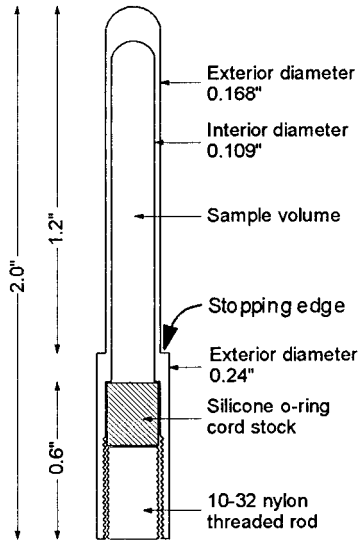

FIG. 4. Schematic diagram of the liquid sample shuttle. The body of the shuttle is made from Delrin and the liquid seal is made with silicone O-ring cord stock.

intensity losses when transit times increase. The signal loss is exponential in the shuttle transit time while the signal loss caused by a smaller volume is approximately linear in the volume. Thus, we choose to minimize transit times. This design permits study of liquids for many shuttle excursions from high to low fields and back again. An excess of 500,000 round trips before failure have been achieved with this design.

The 7.93 mm (5/16-in.)-o.d. and 6.35 mm ($\frac{1}{4}$-in.)-i.d. sample shuttle tube is made of grade XX Garolite, a strong but not brittle paper composite. The shuttle tube seats into a Delrin receiver positioned to center the sample in the low, variable field as shown in Fig. 5 and is sealed by an O-ring to contain the gas pressure. The upper sample stop is represented in Fig.

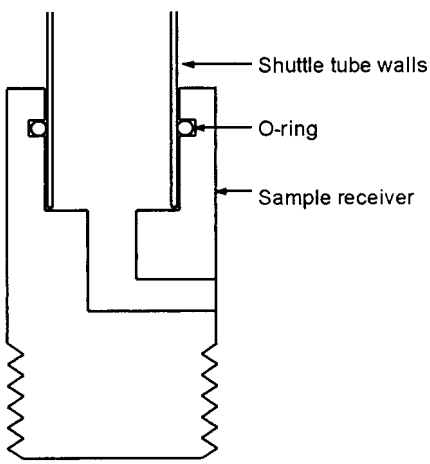

FIG. 5. Schematic diagram of the shuttle tube receiver and sample stop in the evolution field region. The main body is brass, but the sample stop is Delrin, which reduces the sample rebound.

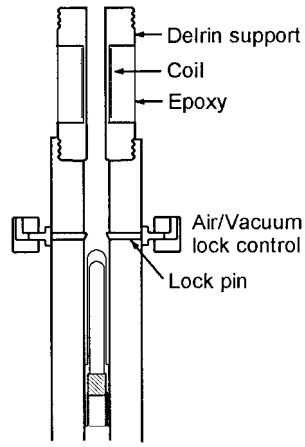

FIG. 6. Schematic diagram of the high-field shuttle tube receiver showing the stop, pneumatically controlled clamping pins, and RF coil.

6, with the sample shuttle shown approaching the resonance region in the high-field magnet. The shuttle receiver housing is made of Delrin; the sample locking pins are made of brass and their position is controlled pneumatically. These pins help guide the sample into the resonance region as it approaches the RF coil, lock it in place when the sample bottom passes, and are retracted pneumatically when a sample excursion to the low field is initiated.

The RF coil is a saddle coil (*10*) cut from 0.00275-in. (0.07-mm)-thick copper tape and is 15 mm long with a 4.76-mm diameter. The coil assembly is constructed by adhering the RF coil to a support machined from Delrin. Wire leads are then soldered to the coil and the surface is potted with 4-mm-thick Ciba Araldite epoxy. Threaded holes in the Delrin support base provide for mechanical adhesion of the epoxy to the Delrin. After the epoxy has cured, the center hole is drilled to the size required to accommodate the shuttle, leaving a 0.2-mm (0.008-in.) Delrin layer on the inside of the resonance region between the RF coil and the sample container.

RELAXATION RATE MEASUREMENT

Relaxation rates for different magnetic fields are determined by polarizing the sample in the preparation field of the superconducting magnet, then moving the sample to the satellite evolution field for a variable time, τ_E, and finally returning the sample to the high field where the magnetization is detected with a standard pulse sequence. The sample experiences a time-varying magnetic field as a consequence of the movement between the two magnetic fields as shown in Fig. 7. The variable time, τ_E, is incremented as in standard relaxation pulse sequences. The sample shuttle trajectories are constant, so that the field excursions that take the spins momentarily to low values of the magnetic field subtract a constant contribution to the signal intensity when the sample returns to the high field.

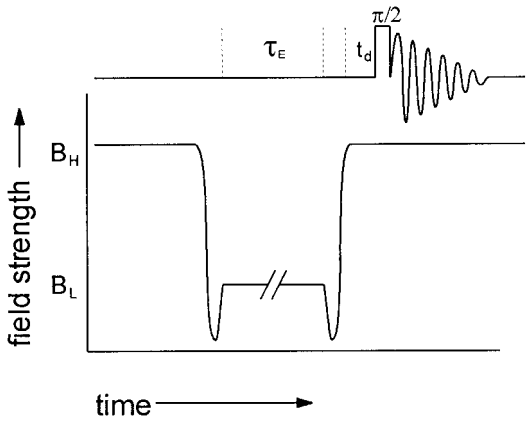

FIG. 7. Schematic diagram of the magnetic field strength experienced by the sample as a function of time during a measurement of the relaxation time. The sample begins a preparation period in the high field during which the magnetization comes to equilibrium. The shuttle to the lower evolution field carries the sample through a near-zero field region between the magnets. After arrival at the low field, the sample magnetization evolves for a variable time, τ_E, after which the sample is moved to the high field. The return path again carries the sample momentarily through the zero-field region before arriving in the high-field resonance region with a delay time t_d before detection.

Measurements have indicated that we may ignore these contributions and fit the relaxation data to a three parameter model:

$$M(\tau_E) = A \exp(-\tau_E/T_1(B_E)) + C.$$

A is proportional to the initial Boltzmann distribution magnetization, and C is a constant resulting from the low-field relaxation effects due to finite sample transit times, low-field magnetization equilibrium values, as well as the settling time in the high field. $T_1(B_E)$ is the relaxation time of the spins observed in the evolution or relaxation field, which is varied systematically thoughout the experiment.

EXAMPLE SOLUTE DISPERSIONS

Multiple Resonance Detection

Figure 8 shows the MRD profiles for water protons as well as methyl protons of dimethyl sulfoxide recorded simultaneously in a serum albumin protein solution. These data demonstrate the advantage of spectral resolution which is achieved using a shimmed high-resolution magnet. Assuming the inflection point at 1 MHZ is a good approximation of the correlation time we see a rotational correlation time of 135 ns reported by both the dimethyl sulfoxide and water protons. The inflection frequency reports the rotational motion of the protein or protein aggregates in the concentrated solution as discussed extensively by others (*11–13*). The similar dispersion in the methyl protons of the cosolvent demonstrates that the rapid exchange of labile solvent protons is not a requirement of the solvent coupling to the protein dynamics in the solution. The relaxation dispersion curves may be understood in terms of a model in which a few solvent binding sites on the protein carry the bulk of the protein-induced relaxation. An interesting feature of these data is the high-frequency tail, which is most apparent in the water data. This feature will be the subject of a separate discussion.

Low-Sensitivity Nuclei: ^{7}Li and ^{111}Cd

Figure 9 shows the MRD profiles for lithium ion in the presence of unilamellar small phospholipid vesicles doped with a nitroxide. The low-field relaxation dispersion may be identified with complex formation between the lithium ion and the nitroxide, leading to a contact or hyperfine coupling between the unpaired electron and the lithium nucleus (*14*). The inflection point corresponds to the correlation time for this coupling which is either the electron relaxation time, T_1, or the residence time for the lithium ion in the complex. Because the electron relaxation times for the nitroxides in lipid environments are generally long, the correlation time for the interaction may be identified with the mean lifetime for the nitroxide–lithium complex at the membrane surface. We note that this lifetime is much longer than that obtained for the nitroxide–lithium complex in a solution without phospholipid vesicles but the formation constant for the complex is substantially smaller.

In the high field region, the lithium ion relaxation rate is linear in the logarithm of the magnetic field strength or the Larmor frequency. This dependence is characteristic of relaxation correlated by translational motions in two dimensions, which has been observed in a variety of contexts (*15, 16*). In this case, the two dimensional character may be imparted by the membrane surface and the associated double layer of coun-

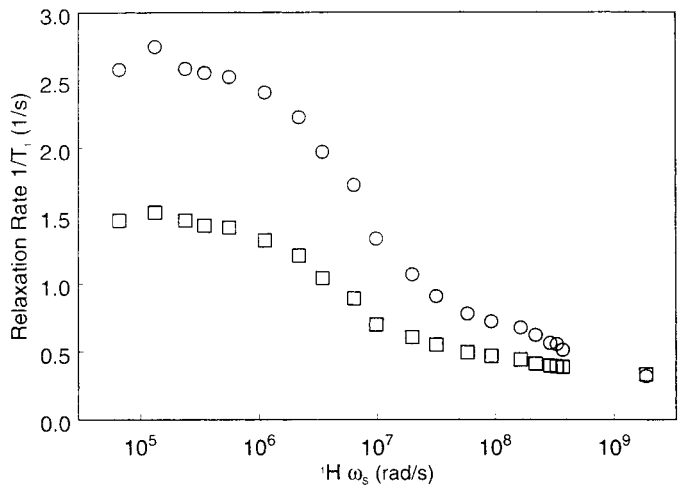

FIG. 8. Magnetic relaxation dispersion profiles for water protons and dimethylsulfoxide (DMSO) protons recorded simultaneously in a 11.7% solution of bovine serum albumin containing 11.7% DMSO and 8.5% H_2O in D_2O at laboratory temperature. The upper curve is for the water protons, the lower curve for the methyl protons.

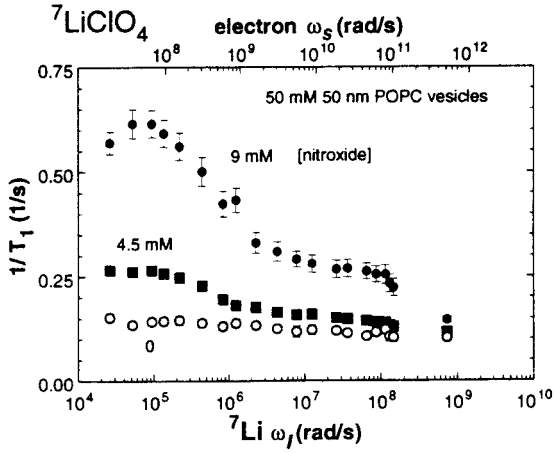

FIG. 9. ^{7}Li magnetic relaxation dispersion profiles obtained for 0.5 M lithium perchlorate aqueous solutions containing 50 mM unilamellar extruded 50 nm POPC phospholipid vesicles, with integrated spin labels 5-doxyl steric acid at 9.5 mM (●) and 4.5 mM (■), total nitroxide concentration. The diamagnetic curve (○) has a small slope thought to derive from diffusion of Li^+ ion at the membrane surface. In the sample containing the paramagnetic spin label, the low field contribution to the relaxation rate can be attributed to a Fermi contact interaction arising from the complexation between the lithium ion and the nitroxide moiety.

terions. The detailed analysis is somewhat involved and will be discussed elsewhere, but it is clear that these experimental approaches will provide a variety of opportunities for defining dynamics of molecules interacting with surfaces, membranes, and membrane-bound functionalities including proteins.

A more challenging sensitivity problem is provided by ^{111}Cd. Data for cadmium relaxed by Mn(II) ion are shown in Fig. 10 which was motivated by the interest in defining the characteristics of like-charge ion pairs thought to be important in a variety of contexts, particularly electron transfer reactions (*17–19*). We have observed complex formation between lithium ion and manganese(II) ion (*20*) and were interested in whether one may observe ion pairing interactions between a 2+ ion and a 2+ ion. The model we used was Mn(II)–Cd(II) because the electron relaxation time for the hexaaquomanganese(II) ion is relatively long. The relaxation dispersion curve shown in Fig. 10 shows contributions to relaxation correlated by both the rotational (dash) and translational (dot) diffusion. The inflection in the cadmium relaxation rate corresponds to a correlation time on the order of 100 ps as inferred from the corresponding electron Larmor frequency. Rotationally correlated motion generates a Lorentzian shaped spectral density and implies the formation of a cation–cation complex with a lifetime at least as long as τ_{rot}. The observation that a cation–cation complex that exists long enough to rotate as a unit, i.e., about 100 ps in the present case, implies that the lifetime of the complex is at least this long. While the Lorentzian form of the MRD data suggests the formation of a complex, the ionic strength is on the order of 10 M so that anion participation in the complex formation is virtually ensured. Nevertheless, the experiment demonstrates the utility of employing paramagnetic centers in the context of a relaxation dispersion experiment, since molecular dynamics on the picosecond time scale may be investigated.

When an electron–nuclear dipole–dipole coupling dominates the nuclear spin relaxation, the relaxation equation includes spectral density terms involving $(\omega_I \pm \omega_S)$, which is well approximated by the electron Larmor frequency. These terms provide dynamical information down to the range of tenths of picoseconds with standard superconducting magnets. Thus, the relaxation dispersion experiment may now provide experimental information about dynamics in solution almost continuously from the range of milliseconds to picoseconds, which significantly overlaps current computational molecular dynamics modeling capabilities.

SUMMARY

The magnetic relaxation dispersion spectrometer assembled here provides reasonably efficient sample transfer between a high-field preparation and detection field and a variable relaxation field which permits acquisition of magnetic relaxation dispersion data on solutes in high resolution. These data sets provide a map of spectral density functions that characterize the fluctuations driving relaxation in the systems and therefore provide a test of the theoretical constructs used to analyze relaxation data. The frequency range that may be probed by these experiments corresponds to time scales on the order of milliseconds to subpicoseconds provided that paramagnetic

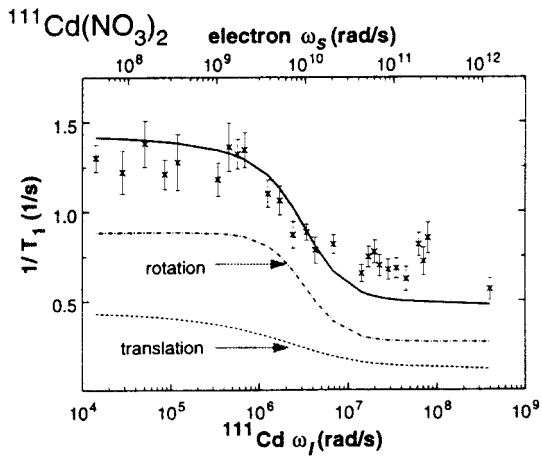

FIG. 10. Cadmium-111 magnetic relaxation dispersion data obtained for a 3.0 M cadmium nitrate solutions in natural isotopic abundance containing 4.5 mM manganese nitrate. The paramagnetic contribution to the cadmium spin–lattice relaxation rate is apparent as the inflection at an electron Larmor frequency of approximately 10^{10} s^{-1}. Several spectra were averaged to overcome the sensitivity problem so that each T_1 value obtained results from 640 measurements. The entire experiment required 5 days. The solid line illustrates the cumulative contributions to relaxation generated by rotational (dash-dot) and translational diffusion (short dash). Deviation of the theoretical line from the data points is due to high ionic strength which has not been accounted for in the theory.

contributions to relaxation may be exploited. The applications of these techniques appear to be extensive.

ACKNOWLEDGMENTS

This work was supported by the University of Virginia and the National Institutes of Health (GM-54067, GM-39309, and GM 34541). This instrument evolved conceptually over a number of years and it is a pleasure to acknowledge helpful input from Ian Walker of GMW, Inc., Niel Munro and the Magnex Company, and Scott Kennedy and Scott Swanson who participated in the formative discussions about this instrument at the University of Rochester.

REFERENCES

1. D. I. Hoult and R. E. Richards, *J. Magn. Reson.* **24,** 71–85 (1975).
2. A. G. Redfield, W. Fite, and H. E. Bleich, *Rev. Sci. Instrum.* **39,** 710–715 (1968).
3. S. H. Koenig and W. E. Schillinger, *J. Biol. Chem.* **244,** 3283–3289 (1969).
4. F. Noack, *Prog. NMR Spectrosc.* **18,** 171–276 (1986).
5. R. Kimmich, *J. Phys. E Sci. Instrum.* **20,** 43–46 (1987).
6. K. H. Schweikert, R. Drieg, and F. Noack, *J. Magn. Reson.* **78,** 77–96 (1988).
7. A. Bielecki, D. B. Zax, K. W. Zilm, and A. Pines, *Rev. Sci. Instrum.* **57,** 393–403 (1986).
8. D. T. Edmonds, M. J. Hunt, A. L. Mackay, and C. P. Summers, *in* "Advances in Nuclear Quadrupole Resonance" (J. S. S. Smith, Ed.), Vol. 1, pp. 145–159 (1974).
9. A. G. Redfield, *Phys. Rev.* **130,** 589 (1963).
10. S. Li, Q. X. Yang, and M. B. Smith, *Magn. Reson. Imaging* **12,** 1079–1087 (1994).
11. S. H. Koenig and R. D. Brown III, *Prog. Nucl. Magn. Reson. Spectrosc.* **22,** 487–567 (1991).
12. R. G. Bryant, *Annu. Rev. Biophys. Biomol. Struct.* **25,** 29–53 (1996).
13. V. P. Denisov, and B. Halle, *Faraday Discuss.* **103,** 227–244 (1996).
14. T. R. J. Dinesen, and R. G. Bryant, *J. Magn. Reson.* **132,** 19–24 (1998).
15. J.-P. Korb, S. Xu, and J. Jonas, *J. Chem. Phys.* **98,** 2411–2422 (1993).
16. J.-P. Korb, M. Whaley, and R. G. Bryant, *Phys. Rev. E.* **56,** 1934 (1997).
17. B. L. Tembe, H. L. Friedman, and M. D. Newton, *J. Chem. Phys.* **76,** 1490–1507 (1982).
18. J. S. Bader, R. A. Kuharshi, and D. Chandler, *J. Chem. Phys.* **93,** 230–236 (1990).
19. R. A Kuharski, J. S. Bader, D. Chandler, M. Sprik, M. Klein, and R. J. Impey, *J. Chem. Phys.* **89,** 3248 (1988).
20. T. R. J. Dinesen, S. Wagner, and R. G. Bryant, *J. Am. Chem. Soc.* **120,** 7004–7009 (1998).